ACS APPLIED MATERIALS & INTERFACES

Research Article

Cite This: ACS Appl. Mater. Interfaces 2019, 11, 8461−8469

www.acsami.org

Exploring the Antibacteria Performance of Multicolor Ag, Au, and Cu Nanoclusters

Shanshan Wang,[†] Yingyi Wang,[†] Yi Peng, and Xiaoming Yang*

College of Pharmaceutical Sciences, Key Laboratory of Luminescent and Real-Time Analytical Chemistry (Ministry of Education), Southwest University, Chongqing 400715, China

Supporting Information

ABSTRACT: Integrating kinds of bactericides as one entirety shows prospect for improving antibacterial efficiency, thus a new type of nanoclusters based on bactericide-directed herein emerged as a combination for achieving a higher antibacterial effect. Specifically, an easily operated approach for preparing bacitracin-directed silver, gold, and copper nanoclusters (AgNCs, AuNCs, and CuNCs, respectively) was proposed. Meanwhile, AgNCs@Bacitracin, AuNCs@Bacitracin, and CuNCs@Bacitracin emitted cyan, yellow, and red colors of fluorescence, respectively, and different sizes and nitrogen contents of these nanoclusters played a critical role for their fluorescence alterations. Significantly, AgNCs@Bacitracin exhibited robust bacteria-killing efficiency than other nanoclusters, owing to its marked damage on the bacterial membrane. Additionally, propidium iodide (PI) staining indicated the bacterial membrane damage of 72.3% to the bacteria population followed by the treatment with AgNCs@Bacitracin, and the introduction of AgNCs@Bacitracin lead to the higher reactive oxygen species (ROS) production, facilitating their attractive antibacterial activity. Moreover, this strategy of developing new nanoclusters broadened the avenues for designing the improved antibacterial materials.

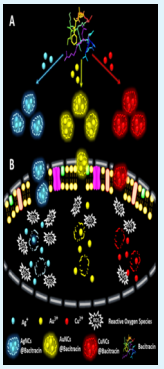

KEYWORDS: *Ag, Au, and Cu Nanoclusters, multicolor, bacitracin-directed, improved antibacterial activity*

1. INTRODUCTION

Bacterial infections have been considered as one of the critical healthcare challenges, and various bacteria exhibit increasing resistance to the existed antibiotics. For this case, developing alternative antibacterial strategies is urgently required.[1−3] Among the alternatives, employing antimicrobial nanomaterials or nanotechnology has been considered as an effective strategy whose rapid advances have indeed provided the opportunities during the past decade.[4,5] Currently, various antibacterial ways based on nanomaterials have been proposed by the virtue of their bactericidal and labeling properties.[6−11]

Extracted from organisms of *B. subtilis*, bacitracin is a type of peptide antibiotic mainly against the Gram-positive bacteria in vitro, which is proved to be water soluble, low toxic, neutral, and stable against heat.[12] It shows the laboratory level activity for the mice infected by the hemolytic streptococcus and the pigs infected by the gas gangrene in vivo.[13,14] Furthermore, utilizing bacitracin for hemolytic streptococcal and staphylococcal infections of human being in clinical has provided the encouraging results.

Defined as isolated particles, metal nanoclusters (MNCs) are composed of a few to tens of atoms and usually exist less than 3 nm.[15,16] Basically, these size particles are generally discrete and exhibit tunable electronic transitions by sizes, leading to their fascinating molecule-like properties such as obvious fluorescence.[17−20] Compared with the routine fluorophores including the organic dyes and semiconductor quantum dots (QDs), their potential applications were possibly restricted because of the weak photostability and toxicity issues, whereas the fluorescent nanoclusters are considered as the promising candidates for designing various bioimaging probes on the basis of their satisfactory photostability, applicable size, and lower toxicity.[21,22] Silver, as one kind of well-known antimicrobial agent, may combine with other antibacterial agents to form silver nanoclusters, thus producing a better antibacterial effect.[23,24] Recently, considerable attention has been directed to the attractive fluorescence performance and diverse values of Ag (Au or Cu) nanoclusters; scarce antibacterial properties of the nanoclusters have been applied.

Hereby, we developed three types of new water-soluble nanoclusters via facile procedures, in which bacitracin served as templates for encapsulating Ag, Au, or Cu atom (Figure 1). Meanwhile, the as-prepared Ag, Au, and Cu NCs@Bacitracin exhibited striking fluorescence such as cyan, yellow, and red, suggesting their potential applications for bio-labeling and beyond. Importantly, we explored the newly developed nanoclusters toward their antibacterial functions. Through the strategy of delivering Ag (Au or Cu) species and bacitracin into a single package, which allowed an efficient and harmonious utilization of nanoclusters and bacitracin, we obtained the enhanced antibacterial effect of both agents, and AgNCs@Bacitracin showed the strongest activity for killing *Staphylococcus aureus* compared with that of other antibacterial agents. We did not only demonstrate the antibacterial performance of the as-prepared nanoclusters but also clarify their mechanism of achieving the improved activity for killing bacteria.

Received: December 25, 2018
Accepted: February 4, 2019
Published: February 4, 2019

DOI: 10.1021/acsami.8b22143
ACS Appl. Mater. Interfaces 2019, 11, 8461−8469

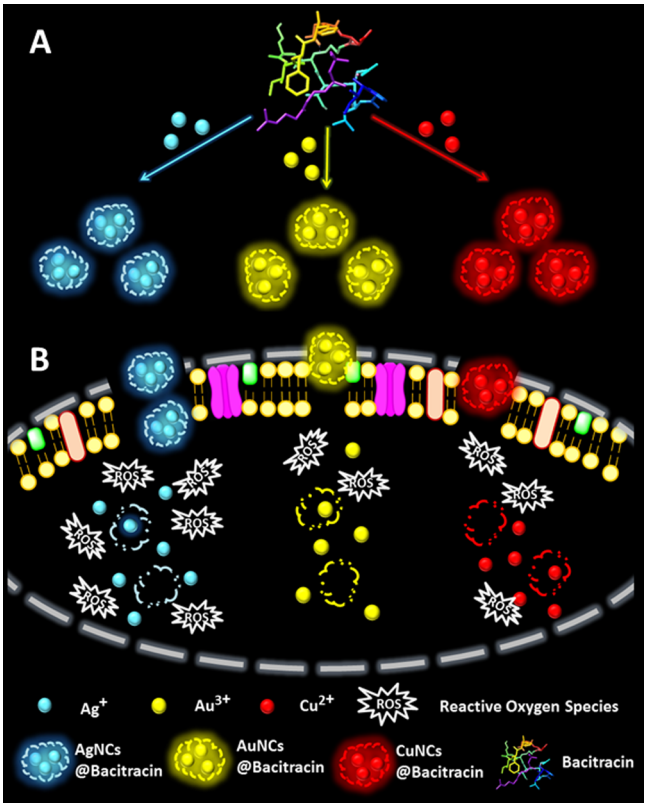

Figure 1. (A) Scheme of preparing AgNCs@Bacitracin, AuNCs@Bacitracin, and CuNCs@Bacitracin. (B) Bacteria treated with AgNCs@Bacitracin, AuNCs@Bacitracin, or CuNCs@Bacitracin.

2. EXPERIMENTAL SECTION

2.1. Chemicals and Materials. Bacitracin and *N*-acetyl-L-cysteine (NAC) were obtained from Aladdin Co., Ltd. (Shanghai, China). Copper sulphate ($CuSO_4$), hydrogen tetrachloroaurate trihydrate ($HAuCl_4$), silver nitrate ($AgNO_3$), propidium iodide (PI), sodium borohydride (98%), and paraformaldehyde (PFA) were purchased from Sigma-Aldrich (Milwaukee, USA). The acids and alkalis that mainly include boric acid (H_3BO_3), phosphoric acid (H_3PO_4), sodium hydroxide (NaOH), hydrazine hydrate ($N_2H_4{\cdot}H_2O$), and sodium chloride (NaCl) were acquired from Dingguo Changsheng Biotechnology Co., Ltd. (Beijing, China). 2′,7′-Dichlorofluorescein diacetate (DCFH-DA) was bought from Nanjing Jiancheng Bioengineering Institute. Methicillin-resistant *S. aureus* (ATCC 6538) were obtained from China General Microbiological Culture Collection Center. Besides, ultrapure water of 18.25 MΩ·cm, produced by an Aquapro AWL-0502-P ultrapure water system (Chongqing, China), was utilized during the whole experimental process.

2.2. Instrumentation. The fluorescent detections were achieved by a Hitachi F-7000 fluorescence spectrophotometer (Tokyo, Japan) with an excitation wavelength of 5 nm and an emission of 10 nm, while the quartz cell is 1 × 1 cm. Next, a Shimadzu UV-2450 spectrophotometer (Tokyo, Japan) was used to obtain absorption spectra. Toward the size distributions, a Zetasizer Nano Dynamic light scattering (DLS) instrument (Malvern, England) was employed. Also, Images of high-resolution transmission electron microscopy (HR-TEM) were taken by a TECNAI G2F20 microscope (Portland, America) at 200 kV. Meanwhile, a ESCALAB 250 X-ray photoelectron spectrometer (XPS) and a Fourier transform infrared (FTIR) spectroscopy (Tokyo, Japan) were applied to explore the elements and chemical groups. The fluorescence quantum yields were determined using Absolute PL quantum yield spectrometer C11347 (Hamamatsu, Japan). Images of the bacterial cells were obtained by a Nikon A1$^+$ confocal microscope (Tokyo, Japan). All pH values of the solutions were detected using a Fangzhong pHS-3C digital pH meter (Chengdu, China), and a DF-101s thermostatic water bath was bought from Gongyi Instrument Co., Ltd (Gongyi, China). Besides, the solution blending was accomplished by vortex mixer QL-901 (Haimen, China), and three-nanocluster powder was produced through lyophilization by PiloFD8-4.3V (Charlotte, USA).

2.3. Synthesis and Purification of AgNCs@Bacitracin, AuNCs@Bacitracin, and CuNCs@Bacitracin. The bacitracin-directed AgNCs, AuNCs, and CuNCs were innovatively synthesized here. Generally, the glassware were first rinsed with aqua regia and further washed by distilled water before use. Also, the magnetic stirring bars were subjected to similar wash steps. To synthesize AgNCs@Bacitracin, 1 mL of bacitracin (13 mg·mL^{-1}) was introduced to 1.6 mL of $AgNO_3$ (17 mM). Subsequently, 200 μL of NaOH (1 M) and 20 μL of $NaBH_4$ (1 mM) were successively added. Then, the previous mixture was incubated for 3.5 h at 37 °C. Similar for AuNCs@Bacitracin, 0.1 g of bacitracin powder dissolved in 3 mL of ultrapure water followed by an addition of 100 μL of $HAuCl_4$ (100 mM). After 3 min, 1 mL of NaOH (1 M) solution was introduced, and the mixture was incubated at 4 °C for 12 h. Again for CuNCs@Bacitracin, 1 mL of bacitracin solution (13 mg·mL^{-1}) and 0.2 mL of $CuSO_4$ (20 mM) were mixed together with stirring for 10 min at 37 °C in a flask. Then, 20 μL of $NaBH_4$ (1 mM) and 60 μL of $N_2H_4{\cdot}H_2O$ were added into the reaction and incubated for 3.5 h with continuous stirring.

Toward purification, AgNCs, AuNCs, and CuNCs aqueous solutions were initially centrifuged at 10000 rpm for 15 min, and the supernatant was filtered by a membrane size of 0.22 μm to remove larger particles. Then, the nanoclusters were obtained through a dialysis membrane (300 MWCO) in deionized water for 24 h. Furthermore, the powder of three nanoclusters was acquired with lyophilization, and their related concentrations of 10 mg·mL^{-1} were obtained by dissolving in ultrapure water for further applications.

2.4. Bacterial Cell Culture. *S. aureus* was initially recovered and cultured in a trypticase soy broth (TSB) medium in a shaker of 37 °C with 180 rpm, and its maintenance was achieved through the growth on TSB agar (15% w/v agar in TSB medium). For each experiment, a single colony of *S. aureus* was selected from the fresh TSB agar plate and subjected to the culture at 37 °C and 180 rpm for 14 h. Finally, the cultured bacteria were introduced for further experiments.

2.5. Nanoclusters Introduced into Bacteria. To identify the antibacterial activity of three nanoclusters against *S. aureus*, the agar diffusion test was performed. In particular, *S. aureus* were spread on agar plates of Luria−Bertani. Then, five aseptic filter papers with AgNCs@Bacitracin, AuNCs@Bacitracin, CuNCs@Bacitracin, bacitracin, and ampicinlin (10 mg·mL^{-1}) were separately placed on the culture plates. Subsequently, these plates were incubated for 16 h with a temperature of 37 °C. Again, we used a Vernier caliper to determine the inhibition diameters, and all the experiments were conducted for three times with a parallel format. Hence, we calculated average values of the inhibition diameters. Next, AgNCs@Papain (10 mg·mL^{-1}), AuNCs@Papain (10 mg·mL^{-1}), CuNCs@Papain (10 mg·mL^{-1}), AgNCs@BSA (10 mg·mL^{-1}), AuNCs@BSA (10 mg·mL^{-1}), CuNCs@BSA (10 mg·mL^{-1}), Ag^+ plus bacitracin (30 μM metal ions and 10 mg·mL^{-1} bacitracin), Au^{3+} plus bacitracin (30 μM metal ions and 10 mg·mL^{-1} bacitracin), and Cu^{2+} plus bacitracin (30 μM metal ions and 10 mg·mL^{-1} bacitracin) were treated similarly.

Growth curves of *S. aureus* with different treatments were plotted. Initially, the cultured *S. aureus* was added into the fresh TSB medium to obtain a concentration of 0.03 with OD600. Next, the previous solutions were separately introduced into five round-bottom tubes with 1000 μL each, and 5 μL of AgNCs@Bacitracin, AuNCs@Bacitracin, CuNCs@Bacitracin, Bacitracin (10 mg·mL^{-1}), or water were added into these tubes. Then, the mixtures were incubated at 37 °C with 180 rpm for 9 h, and their related absorbance at 600 nm was recorded for each hour.

2.6. Membrane Damage of Bacteria. Propidium iodide (PI) was cell impermeable and indicated a high uptake by the dead cells with the damaged membrane, thus leaving the healthy cell unstained. Thereby, PI was employed to trace the membrane damage of the bacterial cell. Additionally, we introduced Hoechst 33342 for staining both the alive and dead population of the bacteria. Specifically, the bacterial cells were

DOI: 10.1021/acsami.8b22143
ACS Appl. Mater. Interfaces 2019, 11, 8461−8469

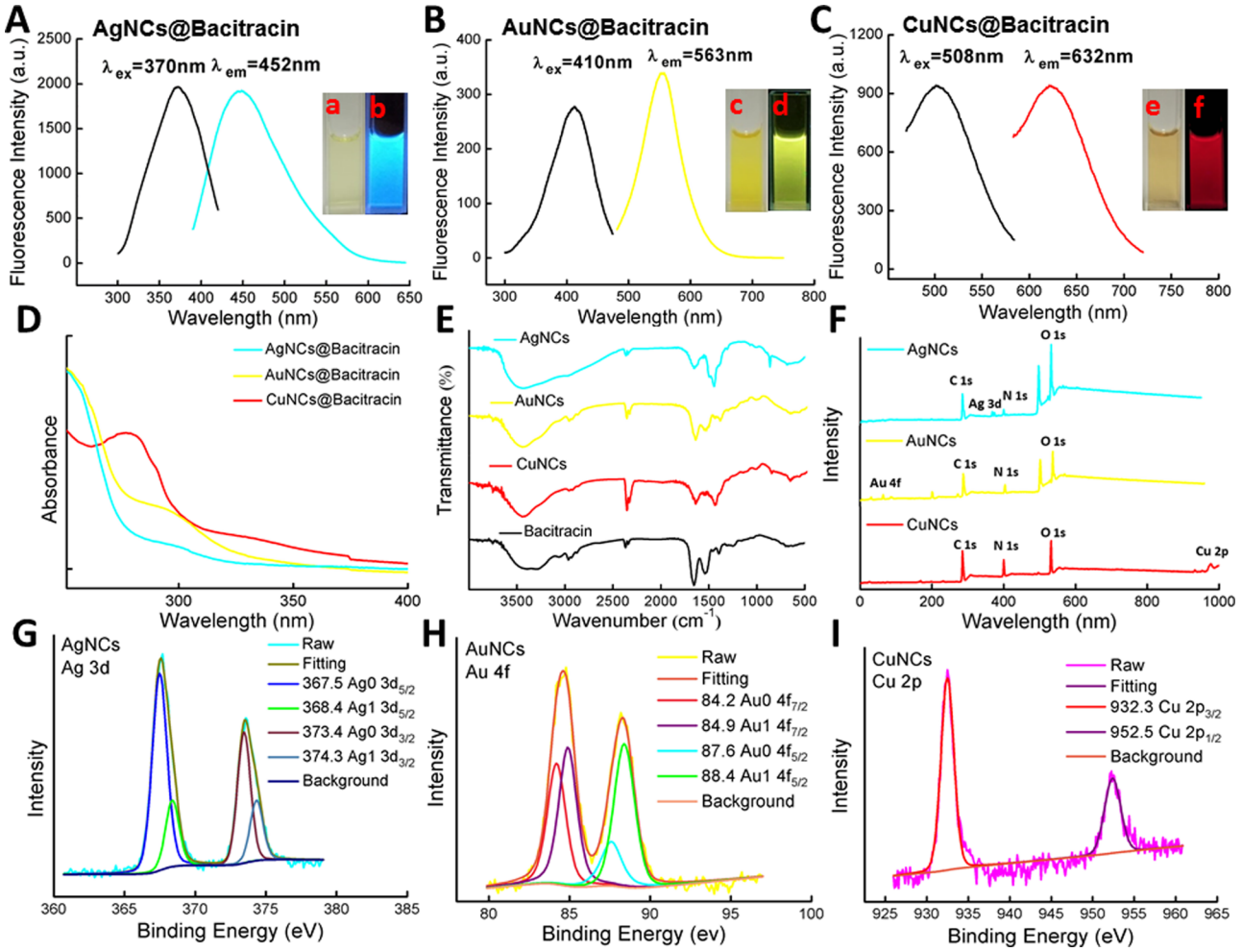

Figure 2. Fluorescence spectra of (A) AgNCs@Bacitracin, (B) AuNCs@Bacitracin, and (C) CuNCs@Bacitracin. (D) UV−vis absorption spectra of AgNCs@Bacitracin, AuNCs@Bacitracin, and CuNCs@Bacitracin. (E) FTIR analyses of bacitracin, AgNCs@Bacitracin, AuNCs@Bacitracin, and CuNCs@Bacitracin. (F) XPS surveys of AgNCs@Bacitracin, AuNCs@Bacitracin, and CuNCs@Bacitracin. (G−I) Binding energy spectra of Ag 3d (AgNCs@Bacitracin), Au 4f (AuNCs@Bacitracin), and Cu 2p (CuNCs@Bacitracin).

first incubated with Ag^+, bacitracin, Ag^+ plus bacitracin, and AgNCs@Bacitracin solutions for 2 h, and then 30 $\mu g \cdot mL^{-1}$ PI was added into each bacterial solution and incubated in the shakers at 37 °C and 180 rpm for 30 min. Later, the bacterial cells were subjected to centrifugation at 5000 rpm for 2 min followed by washing with PBS for three times and resuspended in the PBS as 1 mL. Finally, the bacterial cells were fixed on the slides by 4% paraformaldehyde in PBS for 15 min, and then, 1 $\mu g \cdot mL^{-1}$ Hoechst 33342 solution (Nuclear dye reagent) was added onto the slides and fixed for 30 min. The bacterial cells were observed by laser scanning confocal microscopy, and cell numbers of PI- and Hoechst 33342-stained bacteria were counted. Eventually, the percentage of PI-stained bacteria was calculated through the number of PI stained bacteria divided by that of Hoechst 33342-stained bacteria.[23]

2.7. Reactive Oxygen Species Generation. To investigate the intracellular reactive oxygen species (ROS) concentrations, the bacterial cells were separately treated with 5 μL of AgNCs@Bacitracin, AuNCs@Bacitracin, CuNCs@Bacitracin (10 $mg \cdot mL^{-1}$ for each) for 2 h, and followed by introducing 1 μM DCFH-DA for each, and they were incubated at 37 °C and 150 rpm for 15 min. Subsequently, the bacterial cell suspensions were centrifuged at 5000 rpm for 3 min, washed with PBS for three times, and resuspended in PBS as 1 mL. Then, the fluorescence of the DCF as-produced was recorded with an excitation wavelength of 485 nm, and the relative ROS production level was calculated by normalizing the ROS level of the treated group with that of water treated. As the control, 25 mM *N*-acetyl-L-cysteine (NAC) was separately introduced into three aliquots of bacterial cells, and each was further treated with AgNCs@Bacitracin, AuNCs@Bacitracin, and CuNCs@Bacitracin.[25]

2.8. Injury Model of Mice. Injury models of mice were introduced to further investigate the antibacterial activities of AgNCs@Bacitracin, AuNCs@Bacitracin, and CuNCs@Bacitracin. Particularly, 12 female Kunming mice were divided into four groups (each was3 weeks of age with 18−22 g of weight) and infected with *S. aureus* through a measured bored wound of 36 mm^2. Then, saline AgNCs@Bacitracin (10 $mg \cdot mL^{-1}$), AuNCs@Bacitracin (10 $mg \cdot mL^{-1}$), and CuNCs@Bacitracin (10 $mg \cdot mL^{-1}$) were daubed on the blank band-aids. Again, we monitored the four groups of mice treated with the various band-aids, which were consecutively renewed for 24 h interval. Eventually, the results were photographed during 3 days.

3. RESULTS AND DISCUSSION

3.1. Optimizing Conditions of Synthesis. To obtain optimal conditions of synthesized AgNCs@Bacitracin, AuNCs@Bacitracin, and CuNCs@Bacitracin, more detailed experiments were conducted. As shown in Figures S1−S3, the fluorescence intensities of three nanocluters were varied along different temperatures (Figure S1A), incubation times (Figure S1B), and amounts of $AgNO_3$ (Figure S1C) and bacitracin (Figure S1D) added, suggesting that the preparation of AgNCs@Bacitracin was dependent on the optimization parameters. Finally, at 37 °C for 3.5 h with 20 mM $AgNO_3$

DOI: 10.1021/acsami.8b22143
ACS Appl. Mater. Interfaces 2019, 11, 8461−8469

and, 9 mM bacitracin were determined as the optimum conditions for synthetizing AgNCs@Bacitracin, whereas at room temperature for 1 h with 100 mM $HAuCl_4$ and 80 mM of bacitracin for AuNCs@Bacitracin (Figure S2A−D). Similarly, at 37 °C for 3.5 h with 20 mM $CuSO_{47}$ and 9 mM bacitracin were selected as the applicable conditions for synthesizing CuNCs@Bacitracin (Figure S3A−D).

3.2. Characterization of AgNCs@Bacitracin, AuNCs@Bacitracin, and CuNCs@Bacitracin. According to the particular design, the three metal NCs were prepared in an aqueous solution. Initially, fluorescence spectroscopy was employed to identify their related fluorescent properties. Briefly, the emission peak of AgNCs@Bacitracin emerged at 452 nm with cyan fluorescence under UV light (Figure 2A), whereas AuNCs@Bacitracin showed yellow fluorescent emission at 563 nm (Figure 2B). Likewise, CuNCs@Bacitracin emitted red fluorescence at 632 nm (Figure 2C). Meanwhile, their corresponding excitation spectra for these nanoclusters were separately gained. For AgNCs@Bacitracin, the excitation peak was at 370 nm, and AuNCs@Bacitracin was excitated at 410 nm, whereas CuNCs@Bacitracin was at 508 nm. Again, the absolute PL quantum yields (QY) were separately obtained as 8.3, 5.8, and 3.2% for AgNCs@Bacitracin, AuNCs@Bacitracin, and CuNCs@Bacitracin, respectively, and the lifespan of CuNC@bacitracin was longer than that of both AuNCs@Bacitracin and AgNC@bacitracin (Figure S4). Besides, UV−vis absorption spectra of all three clusters exhibited peaks of 285 nm, which were resulted from the n → π^* transition by C═O (Figure 2D).

Functional groups and components of three clusters were obtained and analyzed by FTIR and XPS. First, surface groups of AgNCs@Bacitracin were investigated with FTIR (Figure 2E). More precisely, a characteristic absorption of 3438 cm^{-1} indicated the O−H stretching vibration and 1708 cm^{-1} for C═O stretching vibration, describing there existed carboxylic groups. Again, the peak at 3412 cm^{-1} proved N−H stretching vibration.[26,27] To identify element components of AgNCs@Bacitracin, three major peaks for C, O, and N were obviously appeared in the XPS survey (Figure 2F), demonstrating that the as-prepared were mainly composed of C (51.86%), O (6.94%), and N (40.01%) as shown in Table 1. Meanwhile, the C 1s band of C 1s spectrum could be divided into four peaks (Figure S5A), referring to sp^2 carbons (C═C, 284.5 eV), sp^3 carbons (C−O/C−N, 285.1 eV), carbonyl carbons (C═O, 287.7 eV), and carboxyl carbons (COOH, 289.4 eV). Also, the N 1s band was divided into three peaks at 398.8, 399.4, and 400.5 eV represent pyridinic-*N*, amino-*N*, and pyrrolic-*N* (Figure S5B), respectively, and the O 1s band contains three peaks at 530.9, 531.6, and 532.7 eV for C═O, C−O−C, and C−OH (Figure S5C), respectively.[28] Altogether, FTIR and XPS data provided the evidence for AgNCs@Bacitracin consisting of both the oxidation and π-conjugated domains. Besides, high polarity and hydrophilicity of AgNCs@Bacitracin were derived from the multiple hydroxyl groups. Similarly, AuNCs@Bacitracin (Figure 2E,F and Figure S5D−F) and CuNCs@Bacitracin (Figure 2E,F and Figure S5G−I) were accordingly investigated by FTIR and XPS, and surface groups of the two clusters were from bacitracin.

Table 1. Elementary Composition and Corresponding Ratios (C, N, and O) of AgNCs@Bacitracin, AuNCs@Bacitracin, and CuNCs@Bacitracin

elementary composition	C (%)	N (%)	O (%)
AgNCs@Bacitracin	51.86	6.94	40.01
AuNCs@Bacitracin	57.64	11.19	29.98
CuNCs@Bacitracin	59.59	16.68	21.47

Additionally, binding energies of Au 4f (84.7 and 88.0 eV) and Ag 3d (368.8 and 374.8 eV) of the two nanoclusters were shown to be approximate to that of the gold (84.1 and 87.6 eV) and silver atoms (368.0 and 374.0 eV) (Figure 2G,H), demonstrating their complete reductions.[29] For Cu 2p spectrum, the absence of the peak at 942 eV clearly excluded the presence of Cu (II) species. Also, binding energies of Cu 2p (932.3 and 952.5 eV) exhibited a valence state that lied at 0 or +1 (Figure 2I), illustrating an acceptable agreement with the previous reports.[30]

To picture these proposed nanoclusters, AgNCs@Bacitracin, AuNCs@Bacitracin, and CuNCs@Bacitracin were visualized by HR-TEM, showing parallel morphology. In detail, most of AgNCs@Bacitracin displayed well-dispersed particles (Figure 3A,B), and their corresponding sizes were measured as 3.2 ± 0.6 nm with a polydispersity index (PDI) of 0.42 (Figure 3C) by DLS, proving a favorable agreement with the data of HR-TEM. Similarly, the majority of AuNCs@Bacitracin were of uniform dispersity with sizes of 4.6 ± 0.8 nm as PDI = 0.57 (Figure 3D−F), and the size of CuNCs@Bacitracin were within a size of 5.5 ± 1.1 nm with a PDI of 0.50 (Figure 3G−I).[31] Thereby, the quantum size effect was responsible for regulating fluorescence emissions of three clusters.[32,33] Through detailed characterization (Table 1), only the particle sizes and nitrogen contents (6.94, 11.19, and 16.68% for AgNCs@Bacitracin, AuNCs@Bacitracin, and CuNCs@Bacitracin, respectively) of three clusters were proved to be distinctly different. These variations were believed to be responsible for the different fluorescence of three nanoclusters.[28,34] Moreover, the current three nanoclusters showed less toxicity for mammalian cells, even though they were incubated with a high dosage amount of 50 $\mu g \cdot mL^{-1}$ for 24 h, clarifying their satisfactory biocompatibility toward the potential applications in vivo (Figure S6A−C).

3.3. Stability of AgNCs@Bacitracin, AuNCs@Bacitracin, and CuNCs@Bacitracin. To investigate fluorescent stabilities of AgNCs@Bacitracin, AuNCs@Bacitracin, and CuNCs@Bacitracin, the related experiments were conducted. First, the fluorescent signal of AgNCs@Bacitracin hardly showed any variation for different reaction times (10, 20, 30, 40, 50, 60, 70, 80, 90, 100, 110, and 120 min) under UV light, indicating their favorable stability (Figure S7A). Also, reaction temperatures of 30, 40, 50, 60, 70, 80, and 90 °C were examined, and in a range of 30−50 °C was the optimal temperature toward the favorable stability (Figure S7B). Besides, fluorescent intensities of AgNCs@Bacitracin exhibited less change along with different concentrations of NaCl (0, 0.1, 0.2, 0.3, 0.4, 0.5, 0.6, 0.7, 0.8, 0.9, and 1.0 M), describing their acceptable tolerance in the hypersaline environment (Figure S7C). Also, proposed AgNCs@Bacitracin was stable upon addition to different kinds of organic solvents, revealing that the fluorescence of AgNCs@Bacitracin was barely affected by the regular organic solvents (Figure S7D).

In a similar manner, the stabilities of AuNCs@Bacitracin and CuNCs@Bacitracin were showed as being satisfactory (Figures S8A and S9A) even under 30−50 °C (Figures S8B and S9B) or in the hypersaline environment (Figures S8C and S9C), and the organic solvents (Figures S8D and S9D) were hardly affected the stability of both AuNCs@Bacitracin and CuNCs@Bacitracin, suggesting that all these three clusters showed favorable stability toward various conditions.

DOI: 10.1021/acsami.8b22143
ACS Appl. Mater. Interfaces 2019, 11, 8461−8469

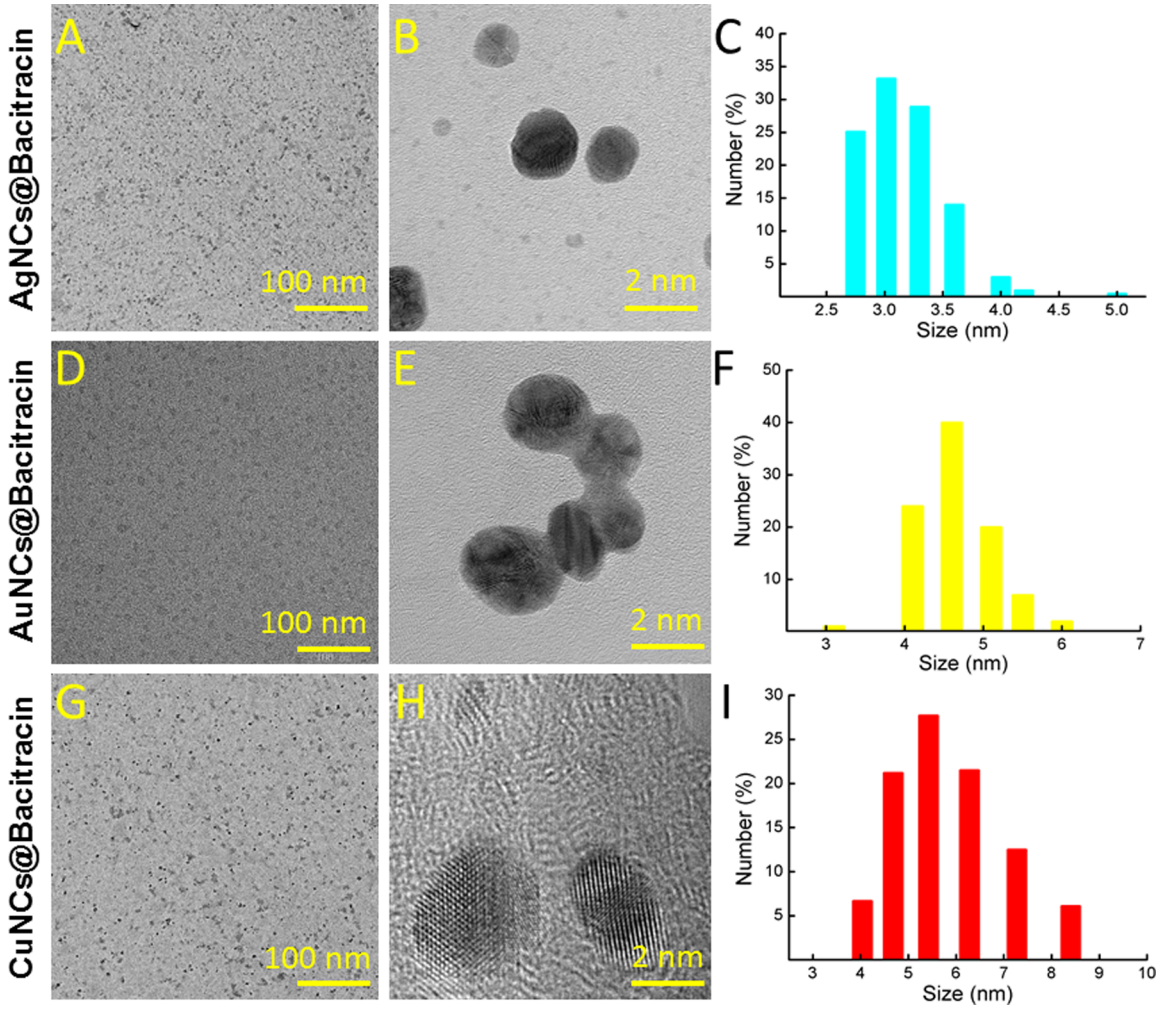

Figure 3. HR-TEM images and DLS analyses of (A−C) AgNCs@Bacitracin, (D−F) AuNCs@Bacitracin, and (G−I) CuNCs@Bacitracin.

3.4. Antibacterial Activity of AgNCs@Bacitracin, AuNCs@Bacitracin, and CuNCs@Bacitracin. To further identify functions and applications of AgNCs@Bacitracin, AuNCs@Bacitracin, and CuNCs@Bacitracin, their antibacterial activities against *S. aureus* were subsequently explored. Particularly, all zones of inhibition treated by AgNCs@Bacitracin displayed a much higher antibacterial activity than that by AuNCs@Bacitracin, CuNCs@Bacitracin, or bacitracin (Figure 4A). Meanwhile, their average inhibition diameters and minimum inhibitory concentrations (MICs) toward *S. aureus* were calculated (Figure 4D and Table S1), and the diameter and MIC of *S. aureus* treated with AgNCs@Bacitracin were 0.82 cm and 6.25 $\mu g \cdot mL^{-1}$, which was obviously longer than that of AuNCs@Bacitracin (0.54 cm, 200 $\mu g \cdot mL^{-1}$), CuNCs@Bacitracin (0.62 cm, 50 $\mu g \cdot mL^{-1}$), or bacitracin (0.50 cm, 200 $\mu g \cdot mL^{-1}$).

To identify interactions of the metal atoms with bacitracin or other proteins, several nanoclusters (AgNCs@Bacitracin, AuNCs@Bacitracin, CuNCs@Bacitracin, AgNCs@Papain, AuNCs@Papain, CuNCs@Papain, AgNCs@BSA, AuNCs@BSA, and CuNCs@BSA) were subjected to the antibacterial experiments. The inhibition diameters and MIC of *S. aureus* treated by three current NCs@Bacitracin showed much higher antibacterial activity than that by three clusters derived from Papain (0 cm, 0 $\mu g \cdot mL^{-1}$) and three clusters based on BSA (0 cm, 0 $\mu g \cdot mL^{-1}$), suggesting their antibacterial functions were mainly derived from the cooperation between bacitracin and the metal atoms (Figure 4B−E). Furthermore, AgNCs@Bacitracin (0.82 cm) displayed a higher antibacterial activity than Ag^+ plus bacitracin (0.68 cm), whereas AuNCs@Bacitracin (0.54 cm) was higher than Au^{3+} plus bacitracin (0.51 cm) and CuNCs@Bacitracin (0.62 cm) higher than Cu^{2+} plus bacitracin (0.59 cm) (Figure 4C−F). To be specific, bacitracin displays the antibacterial activity mainly against the Gram-positive bacteria, whereas BSA and papain indicate a nonantibacterial effect. Thereby, the antibacterial activity of bacitracin was retained while bacitracin cooperated with Ag atoms to form nanoclusters. Taken together, these data demonstrated that silver clusters show the best performance.

3.5. Principle of Antibacterial Activity. To explore the enhanced-antibacterial activity of AgNCs@Bacitracin, growth curves of *S. aureus* treated with AgNCs@Bacitracin, AuNCs@Bacitracin, or CuNCs@Bacitracin (10 $\mu g \cdot mL^{-1}$) were built up. As shown in Figure 5A, a longer lag phase (6 h) was observed for AgNC-treated *S. aureus* than that of AuNC-treated or CuNC-treated *S. aureus* (4 h). Obviously, AgNCs exhibited the enhanced-antibacterial activity compared with AuNCs or CuNCs. Meanwhile, both AuNC- and CuNC-treated *S. aureus* reached the stationary phase over 8 h of growth, and their maximum cell densities showed similarity. These findings suggest that AgNCs shows stronger inhibition for the growth of *S. aureus*.

DOI: 10.1021/acsami.8b22143
ACS Appl. Mater. Interfaces 2019, 11, 8461−8469

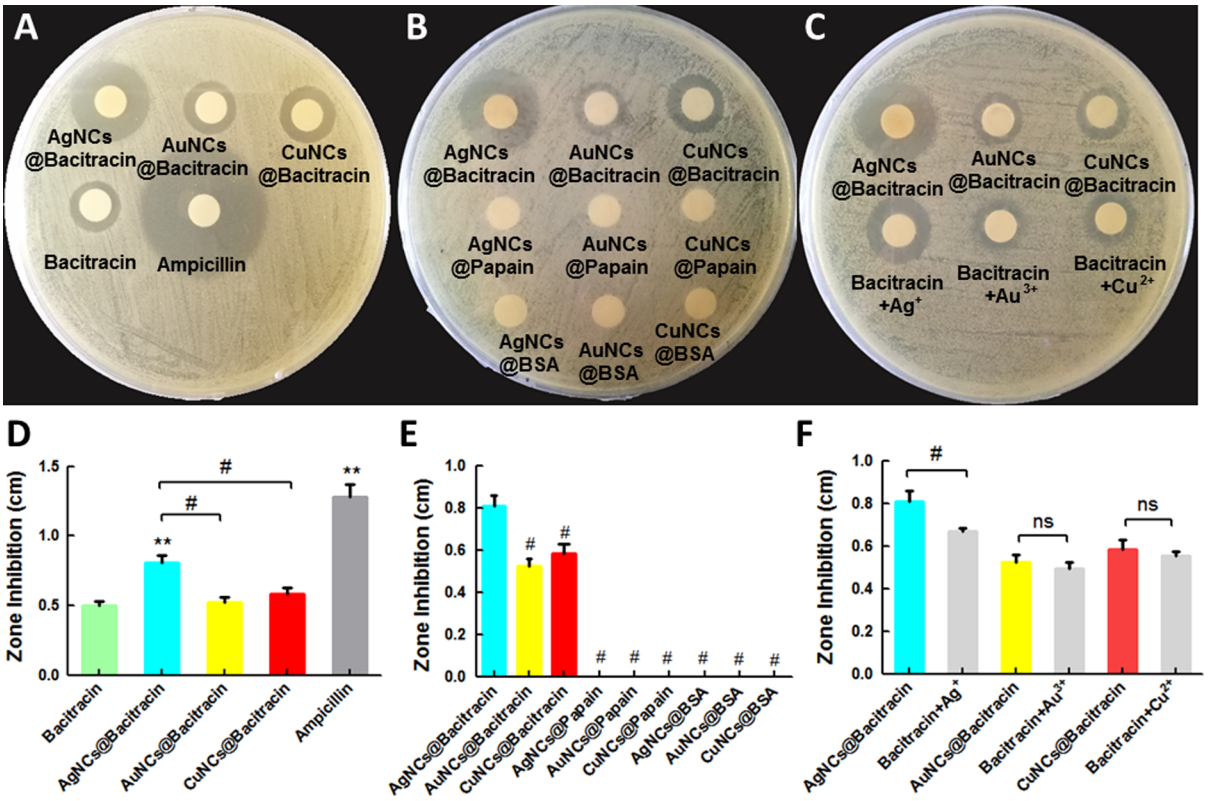

Figure 4. (A) Zone inhibitions of AgNCs@Bacitracin, AuNCs@Bacitracin, CuNCs@Bacitracin, bacitracin, and ampicinlin against *S. aureus*. (B) Zone inhibitions of AgNCs@Bacitracin, AuNCs@Bacitracin, CuNCs@Bacitracin, AgNCs@Papain, AuNCs@Papain, CuNCs@Papain, AgNCs@BSA, AuNCs@BSA, and CuNCs@BSA against *S. aureus*. (C) Zone inhibitions of AgNCs@Bacitracin, AuNCs@Bacitracin, CuNCs@Bacitracin, Ag^+ plus bacitracin, Au^{3+} plus bacitracin, and Cu^{2+} plus bacitracin. (D−F) Related average calculated diameters. Data are mean ± SD, $n = 3$, student t test, $p < 0.05$, asterisk (*) means significant against bacitracin, whereas pound sign (#) as being significant against AgNCs@Bacitracin, $p < 0.05$.

To further illuminate the improved antibacterial activity of AgNCs@Bacitracin, the more detailed investigations for the bacterial membrane damage were performed. Basically, the group treated with water barely damaged the bacterial membrane (Figure 5B). In contrast, the groups with AuNCs@Bacitracin, CuNCs@Bacitracin, or bacitracin treatment separately exhibited 26.6, 30.5, and 33.7% of the bacteria with the damaged membrane. Again, the group treated by Ag^+ or Ag^+ plus bacitracin led to a ratio of 24.3% and 42.1% (Figure S10). In striking contrast, the group of AgNCs@Bacitracin-treated showed a ratio of 72.3% for the membrane-damaged bacteria, suggesting its most powerful activity for antibacteria (Figure 5C). These findings demonstrated that AgNCs@Bacitracin shows the most efficient damage on the bacterial membrane.

Besides, ROSs, which mainly including hydroxyl radicals ($^{\cdot}OH$), superoxide anion radicals ($O_2^{\cdot-}$), and hydrogen peroxide (H_2O_2), were generally refered to the reactive oxygen species of living organisms. As well-known, the excessive production of ROS can cause the damage to the membrane, DNA, and protein of bacteria, thus leading to the cell death. To elucidate the enhanced-antibacterial efficiency of AgNCs@Bacitracin more clearly, we asked whether their antimicrobial efficiency was related to produce ROS. Thereby, we have identified their ROS amounts while *S. aureus* treated with different nanoclusters through a DCFH-DA dye. As shown in Figure 5D, AgNCs@Bacitracin, AuNCs@Bacitracin, and CuNCs@Bacitracin increased the intracellular ROS production. Importantly, AgNCs@Bacitracin induced the maximum increase of ROS, thus inducing the increased cell death for *S. aureus*.[25,35]

Taking the above explorations together, AgNCs@Bacitracin could lead to more broken membranes of bacteria and higher production of ROS, thus facilitating the maximum amount of bacteria cell death. Consequently, AgNCs@Bacitracin shows the highest antibacterial efficiency. Additionally, bacitracin served as the template of the nanoclusters here, formed a package by cooperating with Ag atoms, and also improved the antibacterial activity.[36]

3.6. Band-Aid of Three Nanoclusters Applied for Wounded Mice. To evaluate the antibacterial efficiency of in vivo three metal nanoclusters, Kunming mice wound on their backs were employed as the model.[37] Specifically, the mice were divided to four groups, and each group was treated with band-aids of AgNCs@Bacitracin, AuNCs@Bacitracin, CuNCs@Bacitracin, and Saline. Also, concentrations of three clusters introduced were with 10 $mg{\cdot}mL^{-1}$ each, which was much lower than that of antibiotics commonly used for the wound disinfection. Accordingly, photos of the back-wounded mice of four groups were obtained, and each band-aid was changed every 12 h of interval. During the therapeutic process, recovering situations of the wounds was different, although no change for the body weight was observed. Simultaneously, wounds of mice treated with three band-aids of AgNCs@Bacitracin, AuNCs@Bacitracin, and CuNCs@Bacitracin did not appear with any erythema and edema (Figure 6). Overall, these results suggested that three nanoclusters show the potentiality of serving as the effective antimicrobial nanomaterial, although AgNCs@Bacitracin showed the most powerful activity for killing bacterial cells.

DOI: 10.1021/acsami.8b22143
ACS Appl. Mater. Interfaces 2019, 11, 8461−8469

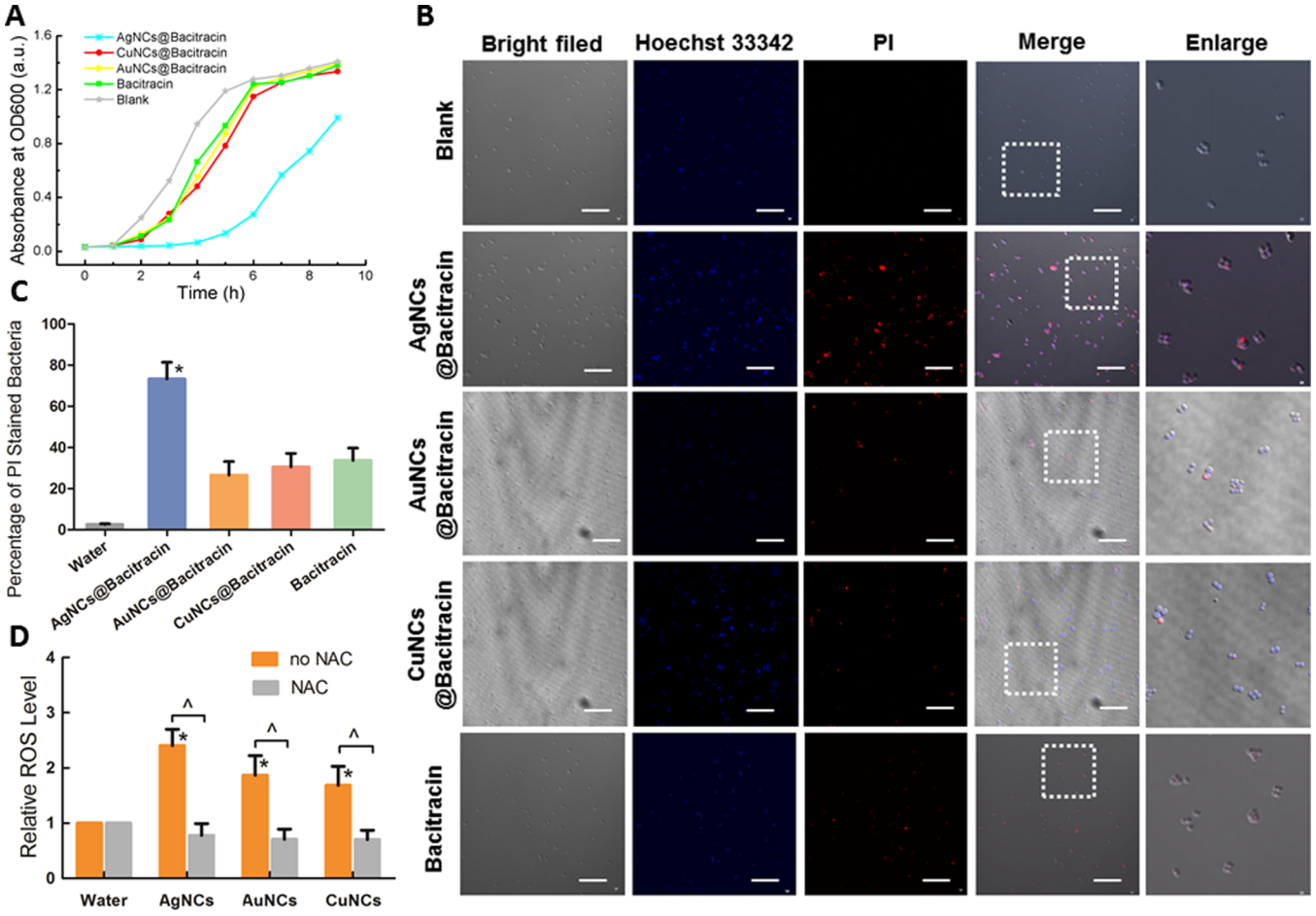

Figure 5. (A) Growth curve of *S. aureus* treated with AgNCs@Bacitracin, AuNCs@Bacitracin, and CuNCs@Bacitracin. (B) Fluorescent photos for the bacteria cells with different treatments (scale bar: 25 μm). (C) Percentage of the bacteria cells stained with PI by introducing water, AgNCs@Bacitracin, AuNCs@Bacitracin, CuNCs@Bacitracin, or bacitracin. $n = 3$, asterisk (*) means significance against the bacitracin-treated group, $p < 0.05$. (D) Relative ROS levels of bacteria treated with AgNCs@Bacitracin, AuNCs@Bacitracin, and CuNCs@Bacitracin, whereas ROS values for two groups treated by water or water with NAC defined as 1, $n = 3$, asterisk (*) means significance against the group treated with water, $p < 0.05$; circumflex accent (^) means significance against non-NAC-treated group, $p < 0.05$.

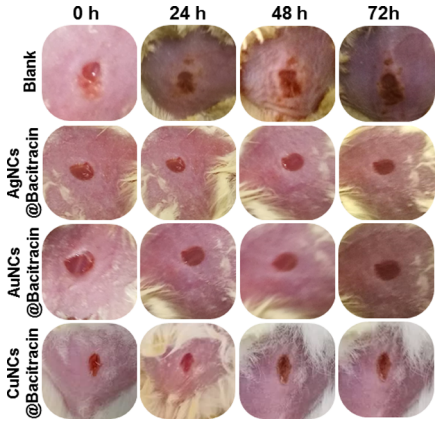

Figure 6. Images of the wounded mice treated with AgNCs@Bacitracin, AuNCs@Bacitracin, CuNCs@Bacitracin, or saline for 0, 24, 48, and 72 h.

4. CONCLUSIONS

In summary, we here innovatively synthesized three antibacterial nanoclusters including AgNCs@Bacitracin, AuNCs@Bacitracin, and CuNCs@Bacitracin with the multicolor fluorescence such as cyan, yellow, and red. Different emissions of the three nanoclusters are proposed originated from differences of the particle sizes and nitrogen contents. Significantly, the as-designed AgNCs@Bacitracin exhibited dramatic bacteria-killing efficiency, which was owing to the hybrid structure of Ag atoms integrated with bacitracin that could effectively damage the bacterial membrane. Besides, the further study suggested that AgNCs@Bacitracin could lead to the higher ROS-production of the bacteria, facilitating their attractive activity over bacteria. More importantly, this strategy broadened the potential for us to design more efficient ways toward the antibacterial substances.

■ ASSOCIATED CONTENT

Supporting Information

The Supporting Information is available free of charge on the ACS Publications website at DOI: 10.1021/acsami.8b22143.

Optimization of syntheses conditions, fluorescence and spectral analyses and images, effects of different organic substances at various conditions, and minimum inhibitory concentration of bacitracin (PDF)

DOI: 10.1021/acsami.8b22143
ACS Appl. Mater. Interfaces 2019, 11, 8461−8469

AUTHOR INFORMATION

Corresponding Author

*E-mail: ming4444@swu.edu.cn. Phone: 86-23-68251225. Fax: 86-23-68251225.

ORCID

Xiaoming Yang: 0000-0002-2514-8672

Author Contributions

†These authors contributed equally.

Notes

The authors declare no competing financial interest.

ACKNOWLEDGMENTS

We gratefully acknowledge the financial support by Fundamental Research Funds for the Central Universities (XDJK2018AC004), Chongqing Research Project of Basic Research and Frontier Exploration (cstc2018jcyjAX0197), Fundamental Research Funds for Innovative Project on Designing and Screening Drug Candidates of Chongqing (cstc2015zdcy-ztzx120003), and Innovative Research Project for Postgraduate Students of Chongqing (CYS18099).

REFERENCES

(1) Costerton, J. W.; Stewart, P. S.; Greenberg, E. P. Bacterial Biofilms: A Common Cause of Persistent Infections. *Science* **1999**, *284*, 1318−1322.

(2) Ebrahiminezhad, A.; Barzegar, Y.; Ghasemi, Y.; Berenjian, A. Green Synthesis And Characterization Of Silver Nanoparticles Using Alcea Rosea Flower Extract as a New Generation Of Antimicrobials. *Chem. Ind. Chem. Eng. Q.* **2017**, *23*, 31−37.

(3) Rai, M.; Yadav, A.; Gade, A. Silver Nanoparticles as a New Generation of Antimicrobials. *Biotechnol. Adv.* **2009**, *27*, 76−83.

(4) Stewart, P. S.; Costerton, J. W. Antibiotic Resistance of Bacteria in Biofilms. *Lancet* **2001**, *358*, 135−138.

(5) Mah, T. F.; O'Toole, G. A. Mechanisms of Biofilm Resistance to Antimicrobial Agents. *Trends Microbiol.* **2001**, *9*, 34−39.

(6) Hancock, R. E. W.; Sahl, H.-G. Antimicrobial and Host-defense Peptides as New Anti-infective Therapeutic Strategies. *Nat. Biotechnol.* **2006**, *24*, 1551−1557.

(7) Lemire, J. A.; Harrison, J. J.; Turner, R. J. Antimicrobial Activity of Metals: Mechanisms, Molecular Targets and Applications. *Nat. Rev. Microbiol.* **2013**, *11*, 371−384.

(8) Steenbergen, J. N.; Alder, J.; Thorne, G. M.; Tally, F. P. Daptomycin: a Lipopeptide Antibiotic for the Treatment of Serious Gram-positive Infections. *J. Antimicrob. Chemother.* **2005**, *55*, 283−288.

(9) Muangsiri, W.; Kirsch, L. E. The Protein-binding and Drug Release Properties of Macromolecular Conjugates Containing Daptomycin and Dextran. *Int. J. Pharm.* **2006**, *315*, 30−43.

(10) Xiu, Z.-m.; Zhang, Q.-b.; Puppala, H. L.; Colvin, V. L.; Alvarez, P. J. J. Negligible Particle-Specific Antibacterial Activity of Silver Nanoparticles. *Nano Lett.* **2012**, *12*, 4271−4275.

(11) Ji, H.; Sun, H.; Qu, X. Antibacterial Applications of Graphene-based Nanomaterials: Recent Achievements and Challenges. *Adv. Drug Delivery Rev.* **2016**, *105*, 176−189.

(12) Godin, B.; Touitou, E. Mechanism of Bacitracin Permeation Enhancement through the Skin and Cellular Membranes from an Ethosomal Carrier. *J. Controlled Release* **2004**, *94*, 365−379.

(13) Engberg, R. M.; Hedemann, M. S.; Leser, T. D.; Jensen, B. B. Effect of Zinc Bacitracin and Salinomycin on Intestinal Microflora and Performance of Broilers. *Poult. Sci.* **2000**, *79*, 1311−1319.

(14) Mascher, T.; Margulis, N. G.; Wang, T.; Ye, R. W.; Helmann, J. D. Cell Wall Stress Responses in Bacillus Subtilis: the Regulatory Network of the Bacitracin Stimulon. *Mol. Microbiol.* **2003**, *50*, 1591−1604.

(15) Zhou, Q.; Lin, Y.; Xu, M.; Gao, Z.; Yang, H.; Tang, D. Facile Synthesis of Enhanced Fluorescent Gold-Silver Bimetallic Nanocluster and Its Application for Highly Sensitive Detection of Inorganic Pyrophosphatase Activity. *Anal. Chem.* **2016**, *88*, 8886−8892.

(16) Lv, S.; Li, Y.; Zhang, K.; Lin, Z.; Tang, D. Carbon Dots/g-C_3N_4 Nanoheterostructures-Based Signal-Generation Tags for Photoelectrochemical Immunoassay of Cancer Biomarkers Coupling with Copper Nanoclusters. *ACS Appl. Mater. Interfaces* **2017**, *9*, 38336−38343.

(17) Zhang, L.; Han, F. Protein Coated Gold Nanoparticles as Template for the Directed Synthesis of Highly Fluorescent Gold Nanoclusters. *Nanotechnology* **2018**, *29*, 165702.

(18) Halawa, M. I.; Gao, W.; Saqib, M.; Kitte, S. A.; Wu, F.; Xu, G. Sensitive Detection of Alkaline Phosphatase by Switching on Gold Nanoclusters Fluorescence Quenched by Pyridoxal Phosphate. *Biosens. Bioelectron.* **2017**, *95*, 8−14.

(19) Gao, G.; Zhang, M.; Gong, D.; Chen, R.; Hu, X.; Sun, T. The Size-effect of Gold Nanoparticles and Nanoclusters in the Inhibition of Amyloid-β Fibrillation. *Nanoscale* **2017**, *9*, 4107−4113.

(20) Xu, M.; Gao, Z.; Wei, Q.; Chen, G.; Tang, D. Label-free Hairpin DNA-scaffolded Silver Nanoclusters for Fluorescent Detection of Hg^{2+} Using Exonuclease III-assisted Target Recycling Amplification. *Biosens. Bioelectron.* **2016**, *79*, 411−415.

(21) Han, L.; Xia, J.-M.; Hai, X.; Shu, Y.; Chen, X.-W.; Wang, J.-H. Protein-Stabilized Gadolinium Oxide-Gold Nanoclusters Hybrid for Multimodal Imaging and Drug Delivery. *ACS Appl. Mater. Interfaces* **2017**, *9*, 6941−6949.

(22) Xu, Y.; Liu, Q.; He, R.; Miao, X.; Ji, M. Imaging Laser-Triggered Drug Release from Gold Nanocages with Transient Absorption Lifetime Microscopy. *ACS Appl. Mater. Interfaces* **2017**, *9*, 19653−19661.

(23) Zheng, K.; Setyawati, M. I.; Lim, T.-P.; Leong, D. T.; Xie, J. Antimicrobial Cluster Bombs: Silver Nanoclusters Packed with Daptomycin. *ACS Nano* **2016**, *10*, 7934−7942.

(24) Sangsuwan, A.; Kawasaki, H.; Matsumura, Y.; Iwasaki, Y. Antimicrobial Silver Nanoclusters Bearing Biocompatible Phosphorylcholine-Based Zwitterionic Protection. *Bioconjugate Chem.* **2016**, *27*, 2527−2533.

(25) Zheng, K.; Setyawati, M. I.; Leong, D. T.; Xie, J. Antimicrobial Gold Nanoclusters. *ACS Nano* **2017**, *11*, 6904−6910.

(26) Yang, K.; Liu, M.; Wang, Y.; Wang, S.; Miao, H.; Yang, L.; Yang, X. Carbon Dots Derived From Fungus for Sensing Hyaluronic Acid and Hyaluronidase. *Sens. Actuators, B* **2017**, *251*, 503−508.

(27) Zeng, R.; Tang, Y.; Zhang, L.; Luo, Z.; Tang, D. Dual-readout Aptasensing of Antibiotic Residues Based on Gold Nanocluster-functionalized MnO2Nanosheets with Target-induced Etching Reaction. *J. Mater. Chem. B* **2018**, *6*, 8071−8077.

(28) Ding, H.; Yu, S.-B.; Wei, J.-S.; Xiong, H.-M. Full-Color Light-Emitting Carbon Dots with a Surface-State-Controlled Luminescence Mechanism. *ACS Nano* **2016**, *10*, 484−491.

(29) Zhou, S.; Zhang, M.; Yang, F.; Wang, F.; Wang, C. Facile Synthesis of Water Soluble Fluorescent Metal (Pt, Au, Ag and Cu) Quantum Clusters for the Selective Detection of Fe^{3+} Ions as Both Fluorescent and Colorimetric Probes. *J. Mater. Chem. C* **2017**, *5*, 2466−2473.

(30) Yang, X.; Feng, Y.; Zhu, S.; Luo, Y.; Zhuo, Y.; Dou, Y. One-step Synthesis and Applications of Fluorescent Cu Nanoclusters Stabilized by L-cysteine in Aqueous Solution. *Anal. Chim. Acta* **2014**, *847*, 49−54.

(31) Wang, Y.; Wang, S.; Lu, C.; Yang, X. Three Kinds of DNA-directed Nanoclusters Cooperating with Graphene Oxide for Assaying Mucin 1, Carcinoembryonic Antigen and Cancer Antigen 125. *Sens. Actuators, B* **2018**, *262*, 9−16.

(32) Tao, Y.; Li, M.; Ren, J.; Qu, X. Metal Nanoclusters: Novel Probes for Diagnostic and Therapeutic Applications. *Chem. Soc. Rev.* **2015**, *44*, 8636−8663.

(33) Zhang, L.; Wang, E. Metal Nanoclusters: New Fluorescent Probes for Sensors and Bioimaging. *Nano Today* **2014**, *9*, 132−157.

(34) Jiang, K.; Sun, S.; Zhang, L.; Lu, Y.; Wu, A.; Cai, C.; Lin, H. Red, Green, and Blue Luminescence by Carbon Dots: Full-Color Emission Tuning and Multicolor Cellular Imaging. *Angew Chem., Int. Ed.* **2015**, *54*, 5360−5363.

DOI: 10.1021/acsami.8b22143
ACS Appl. Mater. Interfaces 2019, 11, 8461−8469

(35) Yuan, X.; Setyawati, M. I.; Leong, D. T.; Xie, J. Ultrasmall Ag^{+}-rich Nanoclusters as Highly Efficient Nanoreservoirs for Bacterial Killing. *Nano Res.* **2014**, *7*, 301−307.
(36) Martinez-Castanon, G. A.; Nino-Martinez, N.; Martinez-Gutierrez, F.; Martinez-Mendoza, J. R.; Ruiz, F. Synthesis and Antibacterial Activity of Silver Nanoparticles with Different Sizes. *J. Nanopart. Res.* **2008**, *10*, 1343−1348.
(37) Miao, H.; Zhong, D.; Zhou, Z.; Yang, X. Papain-Templated Cu Nanoclusters: Assaying and Exhibiting Dramatic Antibacterial Activity Cooperating with H_2O_2. *Nanoscale* **2015**, *7*, 19066−19072.

DOI: 10.1021/acsami.8b22143
ACS Appl. Mater. Interfaces 2019, 11, 8461−8469